Available online at www.sciencedirect.com

ScienceDirect

Ceramics International 42 (2016) 4539–4545

CERAMICS INTERNATIONAL

www.elsevier.com/locate/ceramint

Novel ozone gas sensor based on ZnO nanostructures grown by the microwave-assisted hydrothermal route

L.S.R. Rocha[a,*,1], C.R. Foschini[c,2], C.C. Silva[a,1], E. Longo[b], A.Z. Simões[a,1]

[a]*Universidade Estadual Paulista- Unesp-Faculdade de Engenharia de Guaratinguetá, Av. Dr. Ariberto Pereira da Cunha, 333, Bairro Pedregulho, CEP 12516-410 Guaratinguetá-SP, Brazil*

[b]*Laboratório Interdisciplinar em Cerâmica (LIEC), Departamento de Físico-Química, Instituto de Química, UNESP, CEP: 14800-900 Araraquara, SP, Brazil*

[c]*Universidade Estadual Paulista, UNESP, Faculdade de Engenharia de Bauru, Dept. de Eng. Mecânica, Av. Eng. Luiz Edmundo C. Coube 14-01, 17033-360 Bauru, SP, Brazil*

Received 18 October 2015; received in revised form 25 November 2015; accepted 26 November 2015
Available online 30 November 2015

Abstract

Good quality ZnO nanostructures were obtained by the microwave-assisted hydrothermal synthesis, at low reaction temperatures, using zinc acetate as the starting precursor. X-ray diffraction confirmed the crystallinity of the ZnO nanostructures, which resulted free of impurities. Field emission gun scanning electron microscopy analysis revealed that the ZnO nanostructures crystallized at 120 °C were more homogeneous and had a constant diameter along the entire wire length, exhibiting an ideal defect density that favors the gas sensing response. A new ozone gas sensor based on these nanostructures was evaluated at low exposure times (15 s) by recording the change in the film resistance. The ZnO nanostructures showed good sensitivity even at low ozone concentration (100 ppb), and fast response and short recovery time at 200 °C, demonstrating great potential for a variety of applications. Two main effects were observed: the first one is intrinsic to that of the sample, while the second is a consequence of the surface and interface complex cluster defects, which produce extrinsic defects.

Keywords: A. Powders: chemical preparation; B. Defects; D. ZnO; E. Sensors

1. Introduction

ZnO is an important multifunctional material with an intrinsic *n-type* semiconducting character; recently, it has become the subject of intensive scientific research owing to its unique properties, which enable its effective application in various devices, including light-emitting diodes, nanolasers, piezoelectric devices, antibacterial agents, solar cells, and gas sensors [1–5]. ZnO-based gas sensors have attracted attention because of their high chemical stability, non-toxicity, low cost and fabrication simplicity, as well as the high potential in detecting volatile gases [6–7]. O_3, which is a gas with a high oxidation potential, is an energy rich and highly unstable form of oxygen, and has been extensively applied in several areas, from medicine to drinking water treatment [8–9], assisting in the destabilization and aggregation of particles by several mechanisms, as previously reported [10]. This allotropic molecule is one of the most important gases in the stratosphere because of its ability to filter ultraviolet (UV) rays, which is crucial for the biological balance of the biosphere [11]. On the other hand, when its level exceeds a certain threshold value (higher than 120 ppb, in accordance with the European Guidelines), the exposure to this gas becomes hazardous to human health, as it causes headache, burning eyes, respiratory irritation, and lung damage [12–13]. Therefore, the measurement and continuous monitoring of O_3 levels are of critical importance [14]. Notably, gas sensors require a porous microstructure with a small particle size, to yield a large specific surface area [15]. The sensitivity and response time of ZnO-based sensors strongly depend on the porosity of the material, which is related to certain synthesis parameters, e.g.,

*Corresponding author.
E-mail address: drleandrosrr@gmail.com (L.S.R. Rocha).
[1]Phone +55 12 3123 2765.
[2]Phone +55 14 3103 6119.

http://dx.doi.org/10.1016/j.ceramint.2015.11.145
0272-8842/

the temperature. The predominant electrical characteristics of the semiconductor oxides can be classified according to the resistance change direction relative to the oxidant atmosphere. This classification is related to the intrinsic conductivity type of the semiconductor oxides, which is determined by the nature of the dominant charge carriers; i.e., electrons or holes. In addition, in *n*-type semiconductor oxides, the conductance depends on the oxygen partial pressure, and it decreases when the oxygen partial pressure increases (the inverse occurs in *p*-type semiconductor oxides) [16–17]. In recent years, owing to its many advantages such as rapid heating, low reaction temperatures, homogeneous thermal transmission, and phase purity with superior yield, the microwave hydrothermal route has been used for the synthesis of nanostructured ZnO with several applications within the last years [18–21]. In the microwave process, the heat, which is generated inside the material by the interaction between wave and matter, causes an inversion of the temperature gradient [22]. Thus, owing to these characteristics, the microwave evaporation– final product. To the best of our knowledge, until now, the gas sensing properties of ZnO obtained by the microwave-assisted hydrothermal (MAH) route have never been evaluated, in relation to O_3. In particular, n-type semiconductors including SnO_2, TiO_2, Fe_2O_3, and ZnO have been extensively used for the detection of reducing gases such as CO, CH_4, and alcohol [23–26]. In this paper, we report the sensing properties of one-dimensional ZnO nanocolumn-like structures for O_3; the ZnO nanostructures were obtained by the (MAH) method, which provided extremely large surface areas.

2. Experimental procedure

ZnO nanostructures were synthesized by the MAH route. Zinc acetate dehydrate ($((CH_3CO_2)_2Zn \cdot 2H_2O)$) with 99.9% purity (Aldrich) was dissolved in distilled water under constant stirring for 10 min at 50 °C, forming a solution with $[Zn^{2+}]=0.5$ mol L^{-1}. Subsequently, 2 M KOH (Merck) was slowly added, as the mineralizer agent, until pH 8, to promote the formation of *wurtzite* structure without surface heterogeneities [27]. The resulting solution was transferred into a sealed Teflon autoclave and placed in a hydrothermal microwave oven (2.45 GHz, maximum power 800 W). The system was heat treated at 120 °C and 140 °C, separately, for 8 min, with a heating rate fixed at 10 °C/min. The autoclave was naturally cooled to room temperature. The solutions were centrifuged for 30 min at 2000 rpm, dried at 100 °C in an oven for 24 h, and collected for morphological, structural, and sensing characterizations. The obtained products were characterized by X-ray diffraction (XRD) using a diffractometer (Rigaku-DMax/2500PC, Japan) with Cu-K_α radiation ($\lambda=1.5406$ Å) in the 2θ range of 20–80° at 0.2°/min, Fourier transform infrared (FT-IR) spectroscopy (Bruker Equinox 55, Germany), impedance spectroscopy with a Parstat 2263 system (UNMDP, Argentina), and field emission gun scanning electron microscopy (FEG-SEM: Zeiss Supra 35-VP, Germany). Furthermore, the gas sensing properties of the structures were analyzed. The ZnO crystallite size (d) was calculated using the Scherrer equation $d=k\lambda/\beta \cos\theta$, where k is a constant, λ is the wavelength of the X-rays, and β is the full width at half maximum of the highest intensity reflections measured from a slow scan, in which θ is the diffraction angle of the main peak. To better understand the O_3 sensing properties, which were determined at 1 V and 200 °C, the ZnO nanostructures were dispersed in isopropyl alcohol by an ultrasonic cleaner for 30 min; the suspension was then dripped onto a SiO_2/Si substrate containing 100-nm-thick Pt electrodes separated by a distance of 50 mm. The sample was heat treated for 2 h at 500 °C in an electric furnace in air. The sensor sample was inserted into a test chamber for the control of the temperature at a fixed O_3 concentration. The O_3 gas was formed by oxidation of oxygen molecules of dry air (8.3 cm^3 s^{-1}) with a calibrated pen-ray UV lamp (UVP, model P/N 90-0004-01), obtaining an O_3 concentration of 100 ppb. The dry air containing O_3 was blown directly onto the sensor placed on a heated holder. The applied dc voltage was 1 V, and the electrical resistance was measured using a Keithley (model 6514) electrometer.

3. Results and discussion

Fig. 1 shows the XRD diffraction pattern of ZnO crystallized at 120 °C and 140 °C for 8 min using the MAH route. No significant changes were observed in the XRD pattern with the increase of the crystallization temperature. All diffraction peaks could be indexed to the ZnO hexagonal wurtzite structure (space group: P63mc (186); $a=0.3249$ nm, $c=0.5206$ nm; JCPDS card 036-1451) [28]. The peak intensities relative to the background signal showed the hexagonal phase of products and the high crystallinity of the main phase. No other peaks related to impurities were present. Besides the main phase, peaks coming from the substrate were also evident in the pattern. The intense peaks in the XRD pattern of the powdered sample treated at 120 °C clearly revealed the formation of the ZnO hexagonal wurtzite phase with a

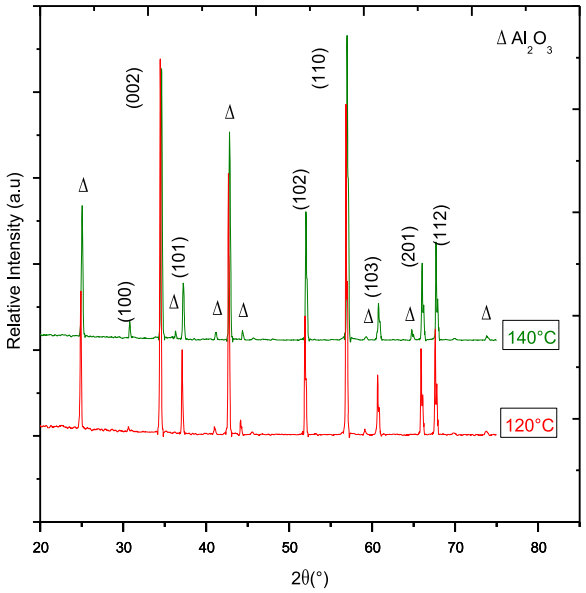

Fig. 1. X-ray diffraction pattern of the ZnO nanostructures obtained with the hydrothermal microwave method after 8 min at 120 °C and 140 °C.

prominent (002) plane. This is the most stable phase of ZnO. Besides, the hydrothermal reaction caused the conversion of $((CH_3CO_2)_2Zn \cdot 2H_2O)$ into ZnO. The nanocrystallites were oriented along the *c* axis, [002] direction. The narrow peaks indicated good sample crystallinity, demonstrating that the ZnO nanocolumns obtained after 8 min using the MAH process had a long-range periodicity. The average crystallite sizes calculated by the Debye–Scherrer method were around 7.03 and 8.80 nm for a soaking time of 8 min at 120 and 140 °C, respectively. Clearly, the crystallization temperature affects the ZnO crystal growth. As the average diffusion distance for the diffusing solute is short and the concentration gradient is steep in concentrated solutions, a considerable amount of diffusing material passes through a unit area per unit time. The use of zinc acetate dehydrate provides a clear evidence that ZnO was formed instead of $Zn(OH)_x$, as this salt is easily dissociable in few milliliters of water, and the friable mass (Zn^{2+}) after the acid treatment, reacted spontaneously with the mineralizer to produce a highly exothermic reaction. When zinc acetate dehydrate is used as the precursor salt and is dissolved with an acid, the Zn^{2+} ion is oxidized to Zn^{3+}, and then the acidic mass reacts exothermically with the mineralizer, forming a by-product salt (KNO_3) that surrounds the hydroxide product. In oxidizing atmospheres, dehydration occurs, converting the hydroxide intermediate to oxide. In the MAH methods, the conversion to oxide is more rapid owing to the effect of the energetic radiations assisting the transformation of $Zn(OH)_x$ to ZnO.

Fig. 2 shows the FTIR spectral features of ZnO nanostructures crystallized at different temperatures. Strong intense bands at around 3750, 2350, 1650, 1075 and below 700 cm^{-1} were observed. The bands at 3750 and 1650 cm^{-1} correspond to the ν and δ (O–H) modes of (H-bonded) water molecules, respectively. As residual water and hydroxyl groups are usually detected in the as-prepared samples, regardless of the synthesis method used [29–30], further heat treatment is necessary for their elimination. Notably, the hydroxylation of metal ions and the deprotonation can be accelerated by raising the solution temperature or pressure. In hydrothermal microwave processing, the high-frequency electromagnetic radiation interacts with the permanent dipole of the liquid (H_2O), causing the molecular rotation and consequent rapid heating. Similarly, permanent or induced dipoles in the dispersed phase cause rapid heating of the particles. This results in a reaction temperature in excess of the surrounding liquid-localized superheating [31]. The FT-IR spectrum also exhibits a strong broad band below 700 cm^{-1}, ascribed to the δ (Zn–O–Zn) mode [32]. Specifically, the strong absorptive peaks at 400–600 cm^{-1} were attributed to the Zn–O stretching and bending vibrations, which are characteristic of the tetrahedral ZnO_4 groups. The traces of carbonate at ~2350 cm^{-1} come from ambient adsorption, in agreement with the literature [32].

FEG-SEM micrographs of ZnO nanostructures obtained at different temperatures are shown in Fig. 3a and b. The MAH synthesis process accelerates the ZnO crystallization, leading to the formation of the material at low temperature and after a short reaction time. Weak aggregations between the particles were observed, indicating that $Zn(OH)_x$ was transformed to ZnO after hydrothermal treatment, and van der Waal's forces were reduced. Moreover, the distribution in size seemed to be homogeneous, while the structures consisted of ZnO multi-wires with a flower-like shape of ~50–400 nm in width and length, showing a clean surface and a hexagonal cross section with a six-fold pyramidal geometry in the extremity. In the hydrothermal process, the presence of an alkaline medium was found to be essential. During the hydrothermal treatment, Zn

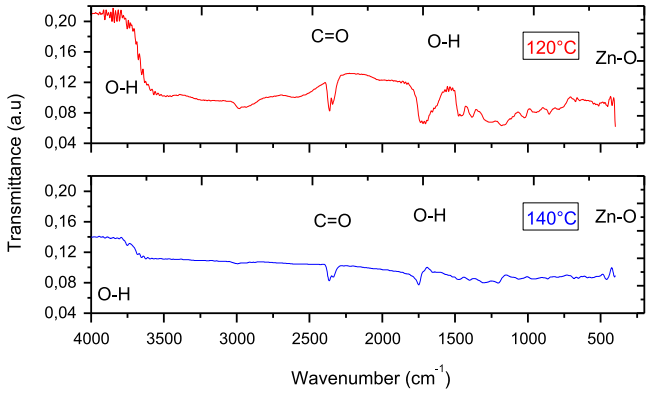

Fig. 2. Fourier transform infrared spectroscopy pattern of the ZnO nanostructures obtained with the hydrothermal microwave method after 8 min at 120 °C and 140 °C.

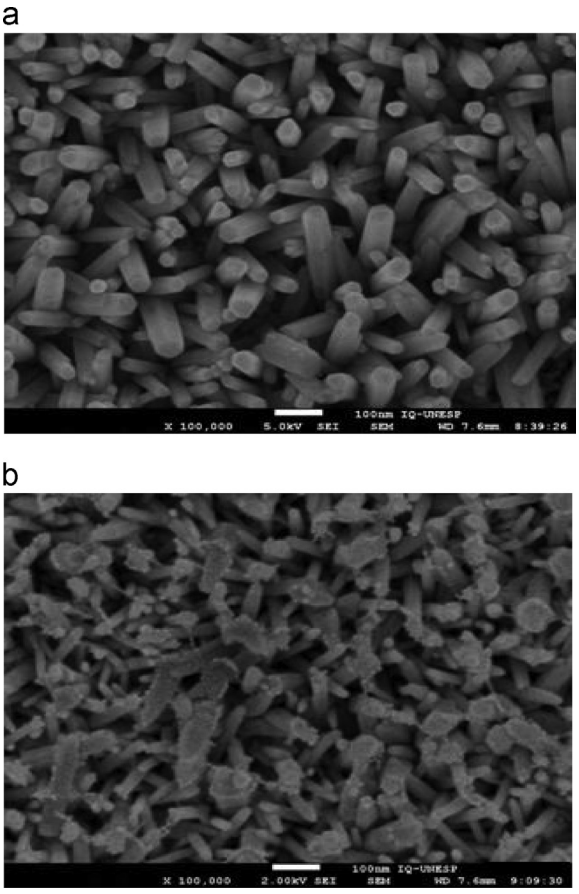

Fig. 3. Field emission gun scanning electron microscopy images of the ZnO nanostructures obtained with the hydrothermal microwave method after 8 min at (a) 120 °C and (b) 140 °C.

hydroxides underwent an attack by the basic medium, dissolving and reacting at higher temperatures and pressures, and finally precipitated as insoluble ceramic oxide particles from the supersaturated hydrothermal fluid. If the temperature and pressure conditions are carefully maintained during the duration of the experiment, neither etching of ZnO crystals nor formation of agglomerates is observed. Therefore, the dissolution and crystallization process continued in supersaturated fluid in such a way that the system was self-stabilizing. The ZnO consists of a non-stoichiometric compound, which contains bulk oxygen vacancies and interstitial oxygen ions that act as donor states. These states permit the adsorption of oxygen. When an oxygen molecule is adsorbed on the ZnO nanostructure surface or at the grain boundaries, it extracts electrons from the conduction band (CB), thus reducing the concentration of the electrons. As the adsorbed oxygen concentration increases, the number of CB electrons further decreases, and the ZnO nanostructures become more resistive. In the microwave-hydrothermal synthesis process, during the rapid growth of particles, different configurations can be produced generating Zn and O vacancies and surface defects, which may be responsible for the different average size distributions of the particles. The samples treated at 120 °C exhibited an average particle diameter of 50 nm, and a particle length of 100 nm. In general, the size of the ZnO wires is uniform; however, the sample treated at 120 °C appeared more homogeneous and showed a constant diameter along the wire length. This sample presented an ideal defect density, which favored the gas sensing response. The obtained ZnO samples presented hexagonally shaped wires of high quality, as shown in the FEG-SEM image. The micrograph revealed that the ZnO morphology was flower-like wire clusters. The clusters were composed of multiple ZnO wires joined together at one end (seed) to form the center, and each grown wire resembled a flower spread outward. Typical flower-like ZnO architectures composed of multiple ZnO wires as swords or pointed wires were observed. The high purity and good crystallinity of the ZnO hexagonal phase demonstrate that the ZnO nanostructures obtained with the MAH method present a long range order or periodicity (completely ordered structure). The facets forming the nanowires and microwires can be polar and non-polar, and a new theoretical analysis of the corresponding values of the surface energy of both polar and non-polar facets of the ZnO system is currently being performed. These results imply that the *c*-axis ((002) direction) is the fast growth direction in ZnO structures, aligned vertically to the page. The particles do not grow beyond a certain threshold magnitude because presumably, at the start of the reaction, a large number of nuclei form in the solution and, as the reaction occurs in a very dilute solution, there is not enough reactant left for the further growth of the particles. The MAH process with KOH as mineralizer showed the efficiency to dehydrate the adsorbed water and decrease the hydrogen bonding effect, leaving weakly agglomerated nanocolumns of ZnO. This behavior indicates that the ZnO nanostructures had a small amount of water adsorbed on the particle surfaces, insufficient to obtain the formation of hydrogen bonds between approaching particles. In the microwave heating process, the introduction of electromagnetic microwave radiation offers significant advantages over the conventional heating method. Furthermore, rapid heating under hydrothermal conditions of pressure and temperature provides higher mobility of the dissolved ions and molecules, and accelerates solid particles to high speed, increasing the collision rate and effective fusion at the collision point [33–34]. Microwave heating led to the formation of crystalline fine particles with a homogeneous distribution at low temperatures and short treatment times. However, at 140 °C, a change in the morphology of the nanostructures was observed. The columnar morphology with its hexagonal geometry, characteristic of the wurtzite phase, was not preserved, and extremely rough surfaces appeared. Owing to the high temperature and pressure reached inside the reaction cell, some structures seemed to coalesce, limiting their application in sensor devices. The Brunauer–Emmet–Teller (BET) specific surface area increased from 90 to 120 m^2/g as the crystallization temperature decreased from 140 to 120 °C. The lower specific surface area of the sample crystallized at 140 °C could be attributed to the agglomeration state of the columnar morphology with extreme roughness.

Impedance spectroscopy is a powerful tool for studying the microstructure characteristics of amorphous semiconductors, ion conductive glasses and transition metal oxides; the impedance Z^* is given by $Z^* = Z' - iZ''$, where Z' and Z'' are the real and complex parts of the impedance spectroscopy, respectively [35]. Once the real and imaginary parts of the impedance at different frequencies are obtained, impedance spectroscopy can be plotted. Impedance spectroscopy provides information on the semiconductor microstructure resistive characteristics due to the resistance of the grains and their boundaries. Fig. 4 shows the impedance spectra in the form of Nyquist plots obtained from the ZnO nanostructures crystallized at different temperatures. The stability of the impedance curves with the increase in operating time reveals the microstructure stability of the semiconductor. The impedance curves of the ZnO sensor consisted of two different arcs (Fig. 4), which indicated the existence of different polarization mechanisms in the films [36–38]. The ZnO sensor crystallized at 140 °C had an irregular impedance curve, which continued to fluctuate randomly over time at fixed temperature (300 °C),

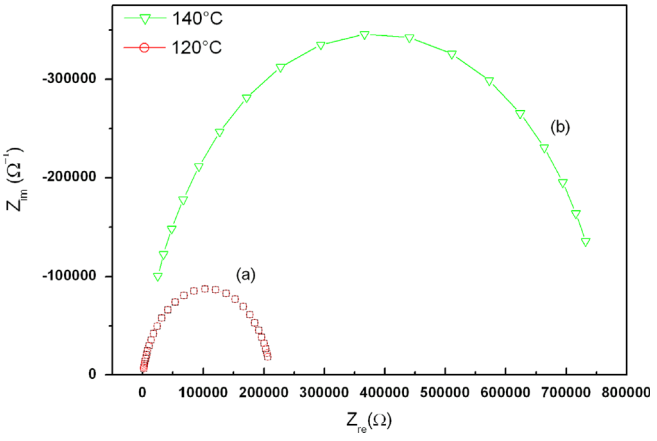

Fig. 4. Cole–Cole plot of complex impedance for ZnO nanostructures obtained with the hydrothermal microwave method after 8 min at 120 °C and 140 °C.

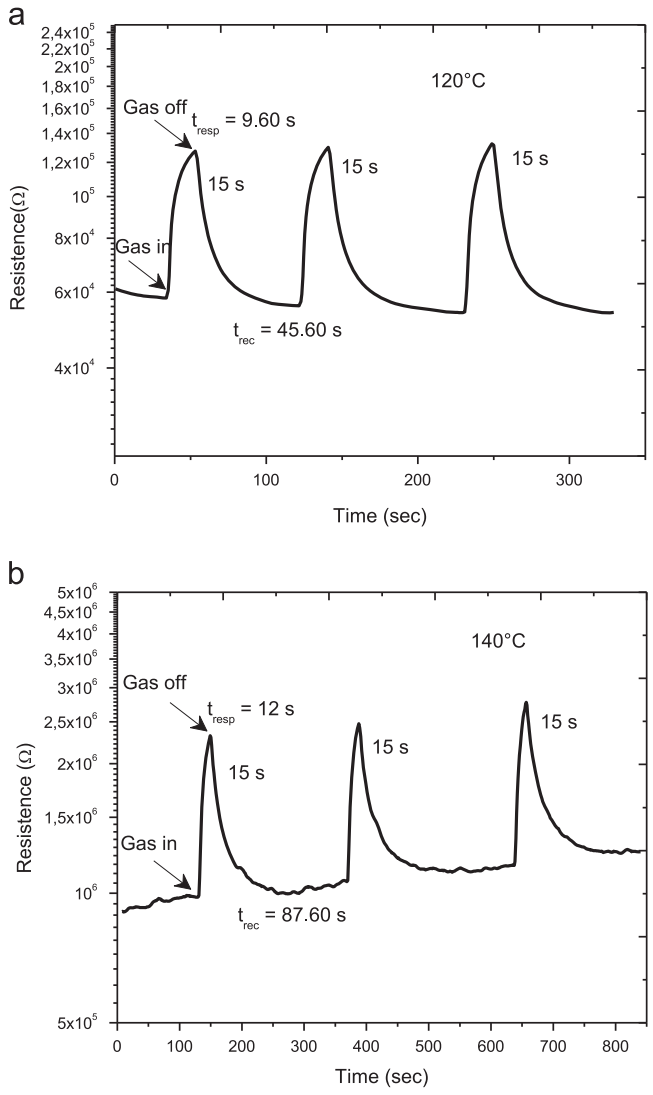

Fig. 5. Ozone gas sensing response for ZnO nanostructures obtained with the hydrothermal microwave method after 8 min at (a) 120 °C and (b) 140 °C; the samples were exposed for 15 s at an operating temperature of 200 °C. The arrows indicate when the ozone gas flow was turned on and off.

thus indicating unstable electrical properties, with complex relaxation mechanisms. The impedance curves of the ZnO sensor crystallized at 120 °C exhibited a homogeneous circular arc and gradually became stable at fixed temperature (300 °C) suggesting stable electrical properties. Therefore, the lower temperature hydrothermal treatment could effectively stabilize the microstructure of the ZnO sensor. A semicircle typically indicates relaxation mechanisms with times closely distributed [39,40]; this behavior has been observed by several authors in different metal oxide nanostructures [41,42]. This mechanism involves charge transfer processes in the material, which has its behavior modeled by an equivalent circuit. A decrease in resistance as the temperature is reduced from 140 °C to 120 °C suggests a decrease in the potential barrier height, due to the introduction of charge carriers, in addition to the increase of electrical conduction at higher temperatures. This decrease is attributed to the thermal excitation of electrons to the CB [43]. In contrast, the diameter of the semicircle increased when the temperature increased from 120 °C to 140 °C, indicating an increase in resistivity, which can be confirmed by the increased band gap of the samples (2.95 and 2.97 eV, respectively).

The resistance response of the ZnO nanostructures was studied at 200 °C under the exposure of 100 ppb of O_3 gas for 15 s; the results are shown in Fig. 5a and b. The samples exhibited good sensitivity at low exposure times as well as total reversibility and good stability of the base line. The ZnO nanostructure based sensors displayed good sensitivity and no evidence of saturation in the evaluated concentration range. Even at low O_3 concentration (100 ppb), the samples obtained at 120 °C and 140 °C exhibited fast response times of 9.6 s and 12 s, respectively, and recovery times of 45.6 s and 87.6 s, respectively, providing results similar to those obtained at high O_3 concentrations. The analysis of the results revealed that the operating temperature of the ZnO nanostructure based sensor is close to that of the WO_3, In_2O_3, and SnO_2 sensors, while the response time is slightly longer than those of the Ag_2WO_4 and SnO_2-based sensors, but significantly shorter than that of the In_2O_3-based sensor [14,44–46]. On the other hand, the recovery time of the ZnO nanostructure based sensor is shorter than those of the WO_3-, In_2O_3- and SnO_2-based sensors. Besides the capability of most metal oxides, such as ZnO, to show sensing properties in oxidizing atmospheres within the ppb range, it can be used to detect reducing analytes, as well as humidity. On this way, A.S.M.I. Uddin et al. [47] obtained an acetylene (C_2H_2) gas sensor consisting of Ag-loaded ZnO nanorods, supported by a polyimide/polytetrafluoroethylene substrate, which exhibited a high response magnitude of 27.2 (at 1000 ppm) with worse response and recovery times (62 and 39 s, respectively), compared to ours, while Galstyan et al. [48] reported the fabrication and sensing properties of ZnO nanostructures, which exhibited relative good sensitivity towards NO_2, H_2, and CH_4 gases, at higher working temperatures (0.37 @ 300 °C, 11.26 @ 400 °C, and 0.1 @ 500 °C, respectively). In addition, Narimani et al. [49] reported the fabrication and characterization of high sensitivity capacitive humidity sensors based on ZnO nanorods grown by means of chemical bath deposition, which demonstrated an extremely long transient time until the result saturates to its final capacity value.

The electrical resistance response is typical of *n*-type semiconductor materials exposed to oxidizing gases. The oxygen species (O_2^- and O^-) chemisorbed on the semiconductor surface decrease the conductivity of the sensor device owing to the lower concentration of free electrons in the CB [44,46]. Remarkably, the ZnO nanostructures obtained at 120 °C displayed good sensitivity, fast response, and short recovery time. We propose two effects regarding the mechanisms concerning the O_3 adsorption in the ZnO nanostructures. The first effect is intrinsic to the sample, and the second is a consequence of the surface and interface complex cluster defects, which produce extrinsic defects. Before the adsorption of O_3, the short and medium range order structural defects generate a non-homogeneous charge distribution in the cell. Upon O_3 adsorption, configuration charges and distorted excited clusters are formed, allowing electrons to become

trapped (O_3^-). We propose a cluster model, based on Kroger–Vink notation, to explain the gas sensor properties of complex metal device of ZnO. In this cluster model, the magnitude and structural order-disorder effects determine their physical properties. We consider ZnO as a non-centrosymmetric oxide where a $[ZnO_4]$ with a 4-fold tetrahedron is the basic constituent unit. The cluster-to-cluster charge-transfer process provides direct insight into the material charge carrier dynamics, with hole polaron trap states localized at oxygen anions in the bulk and on the surface. Oxygen vacancies in a disordered structure with $[ZnO_4]^x/[ZnO_3.Vo^x]$ complex clusters are hole trapping centers and, therefore the gas sensing mechanism can be described by the following equations: The first effect is given by,

$$[ZnO_4]^x - [ZnO_3.Vo^x] \rightarrow [ZnO_4]' - [ZnO_3.Vo^\bullet] \quad (1)$$

$$[ZnO_4]' - [ZnO_3.Vo^\bullet] + O_3 \rightarrow [ZnO_4]' - [ZnO_3.Vo] \ldots - O_3(ads) \quad (2)$$

$$[ZnO_4]' - [ZnO_3.Vo] \ldots - O_3(ads) \rightarrow [ZnO_3.Vo^\bullet] \ldots O_3'(ads) + O^* + O_2'(des) \quad (3)$$

while the second effect can be expressed by

$$[ZnO_4]_o^x - [ZnO_3]_d^x \rightarrow [ZnO_4]_0^{'} - [ZnO_3]_d^\bullet \quad (4)$$

$$[ZnO_4]^{'} - [ZnO_3]_d^\bullet + O_3 \rightarrow [ZnO_4]_o^x - [ZnO_3]_d^\bullet + O_3^{'}(ads) \quad (5)$$

$$[ZnO_4]_o^x - [ZnO_3]_d^\bullet + O_3^{'}(ads) \rightarrow [ZnO_4]_o^x - [ZnO_3]_d^x + O^* + O_2^{'}(des) \quad (6)$$

Good sensor properties, even at relatively low operating temperature (200 °C) [50,51] and an O_3 atmosphere concentration of 100 ppb for 15 s, were observed. Fig. 5a illustrates the response obtained for the ZnO nanostructure synthesized at 120 °C. This sample showed the highest sensitivity to O_3 gas ($m=2.4$) even for a short exposure time (15 s), demonstrating an extremely high value, even at low concentrations, compared with the data in the literature [52]. In addition, this sample showed an *n*-type semiconductor behavior. In the presence of oxidizing gases, electrons in the CB are trapped in the semiconductor, producing negatively charged scattering centers (O^-,O^{2-} ions), which cause an increase of the material strength. Upon suspension of the analyte gas flow (O_3), the scattering centers come in contact with O_2 from the environment and release the trapped electrons, which return to the semiconductor CB, generating a drop in resistance [53]. The ZnO nanostructures synthesized at 140 °C (Fig. 5b) showed good response as O_3 gas sensor, even for a short exposure time (15 s), exhibiting a typical n-type semiconductor behavior and sensitivity (m) of 2.2. The action of the O_3 gas on the ZnO surface can be addressed by (Eqs. (1)–6), which show that the sensor response is quite fast, but the saturation time is different for the adsorption and desorption processes. The faster response is believed to be due to the higher surface area of sensing ZnO nanostructures with smaller particles. In addition, surface defects and configuration affect the detection.

4. Conclusions

This paper presents new results concerning the detection of O_3 by using nanostructured ZnO obtained by the hydrothermal microwave method. The merit of this technology lies in the simplicity of the process, economical energy structures with high efficiency, short duration, accessible auxiliary materials, in addition to the use of non-sophisticated equipment resulting in energy savings, contributing to a more sustainable world. The electrical, morphological and sensing properties of the ZnO nanostructures can be easily modified by controlling the growth regimes and treatment conditions. ZnO nanostructures have a very high sensitivity to O_3 gas. Before the adsorption of O_3, the short and medium range order structural defects generate a non-homogeneous charge distribution in the cell. Upon O_3 adsorption, configuration charges and distorted excited clusters are formed, allowing electrons to become trapped (O_3^-). These materials have shown great potential as novel O_3 gas sensors and displayed good sensitivity to low O_3 concentrations, as well as a good stability, fast response, and short recovery time.

Acknowledgments

The financial support of this research project by the Brazilian research funding agencies CNPq 573636/2008-7, INCTMN 2008/57872-1 and FAPESP 2013/07296-2.

We thank Luis F. da Silva for the ozone gas measurements.

References

[1] L.S.R. Rocha, R.C. Deus, C.R. Foschini, F. Moura, F.G. Garcia, A.Z. Simões, Photoluminescence emission at room temperature in zinc oxide nano-columns, Mater. Res. Bull. 50 (2014) 12–17.

[2] A.K. Pal, D.B. Mohan, Study of NBE emission enhancement with an absence of DL emission from ZnO nanorods through controlled growth on ultra-thin Ag films, Appl. Surf. Sci. 333 (2015) 244–253.

[3] R. Lamba, A. Umar, S.K. Mehta, S.K. Kansal, Sb_2O_3–ZnO nanospindles: a potential material for photocatalytic and sensing applications, Ceram. Int. 41 (2015) 5429–5438.

[4] A. Ghosh, N. Kumari, S. Tewari, A. Bhattacharjee, Structural, electrical and optical studies on ruthenium doped ZnO pellets for device applications, Mater. Sci. Eng.: B 196 (2015) 7–14.

[5] J. Hu, Z. Zhong, F. Zhang, W. Xing, Z.-X. Low, Y. Fan, Coating of ZnO nanoparticles onto the inner pore channel surface of SiC foam to fabricate a novel antibacterial air filter material, Ceram. Int. 41 (2015) 7080–7090.

[6] I. Kortidis, K. Moschovis, F.A. Mahmoud, G. Kiriakidis, Structural analysis of aerosol spray pyrolysis ZnO films exhibiting ultra low ozone detection limits at room temperature, Thin Solid Films 518 (2009) 1208–1213.

[7] C. Shao, Y. Chang, Y. Long, High performance of nanostructured ZnO film gas sensor at room temperature, Sens. Actuators B: Chem. 204 (2004) 666–672.

[8] M.E. Almaz, I.S. Sonmez, Ozone therapy in the management and prevention of caries, J. Formos. Med. Assoc. 114 (2015) 3–11.

[9] M. Sadrnourmohamadi, B. Gorczyca, Effects of ozone as a stand-alone and coagulation aid treatment on the reduction of trihalomethanes precursors from high DOC and hardness water, Water Res. 73 (2015) 171–180.

[10] D.A. Reckhow, P.C. Singer, R.R. Trussell, AWWA Seminar Proceedings-Ozonation: Recent Advances and Research Needs, Ozone as a Coagulant Aid, American Water Works Association, Denver, CO, USA, 1986.

[11] C.G. Nogales, P.H. Ferrari, E.O. Kantorovich, J.L. Lage-Marques, Ozone therapy in medicine and dentistry, J. Contemp. Dental Pract. 9 (2008) 75–84.
[12] L.C. Simões, M. Simões, Biofilms in drinking water: problems and solutions, RSC Adv. 3 (2013) 2520–2533.
[13] C.Y. Wang, R.W. Becker, T. Passow, W. Pletschen, K. Köhler, V. Cimalla, O. Ambacher, Photon stimulated sensor based on indium oxide nanoparticles I: wide-concentration-range ozone monitoring in air, Sens. Actuators B: Chem. 152 (2011) 235–240.
[14] L.F. Silva, A.C. Catto, W. Avansi Jr., L.S. Cavalcante, J. Andrés, K. Aguir, V.R. Mastelaro, E. Longo, A novel ozone gas sensor based on onedimensional (1D) α-Ag_2WO_4 nanostructures, Nanoscale 6 (2014) 4058–4062.
[15] G. Biasotto, M.G.A. Ranieri, C.R. Foschini, A.Z. Simões, E. Longo, M.A. Zaghete, Gas sensor applications of zinc oxide thin film grown by the polymeric precursor method, Ceram. Int. 40 (2014) 14991–14996.
[16] A. Saluja, J. Pan, L. Kerr, E. Cho, S. Hubbard, Gas sensing properties of porous ZnO nano-platelet films, Mater. Res. Soc. Symp. Proc. 1035 (2008) L11-07.
[17] T. Koplin, M. Siemons, C. Valéntin, D. Sanders, U. Simon, Workflow for high throughput screening of gas sensing materials, Sensors 6 (2006) 298–307.
[18] V.K. Ivanov, A.S. Shaporev, F.Y. Sharikov, A.Y. Baranchikov, Hydrothermal and microwave-assisted synthesis of nanocrystalline ZnO photocatalysts, Superlattices Microstruct. 42 (2007) 421–424.
[19] Z. Zhu, D. Yang, H. Liu, Microwave-assisted hydrothermal synthesis of ZnO rod-assembled microspheres and their photocatalytic performances, Adv. Powder Technol. 22 (2011) 493–497.
[20] D. Li, J.-F. Huang, L.-Y. Cao, J.-Y. Li, H.-B. Ouyang, C.-Y. Yao, Microwave hydrothermal synthesis of Sr^{2+} doped ZnO crystallites with enhanced photocatalytic properties, Ceram. Int. 40 (2014) 2647–2653.
[21] E. Mosayebi, S. Azizian, A. Hajian, Synthesis of nanostructured and microstructured ZnO and $Zn(OH)_2$ on activated carbon cloth by hydrothermal and microwave-assisted chemical bath deposition methods, Superllattices Microstruct. 81 (2015) 226–232.
[22] H. Cheng, J. Cheng, Y. Zhang, Q.-M. Wang, Large-scale fabrication of ZnO micro-and nano-structures by microwave thermal evaporation deposition, J. Cryst. Growth 299 (2007) 34–40.
[23] J.H. Yu, G.M. Choi, Selective CO gas detection of CuO- and ZnO-doped SnO_2 gas sensor, Sens. Actuators B: Chem. 75 (2001) 56–61.
[24] Y.S. Choi, C.G. Lee, S.M. Cho, Transparent conducting $Zn_xCd_{1-x}O$ thin films prepared by the sol–gel process, Thin Solid Films 289 (1996) 153–158.
[25] S.M. Hyun, K. Hong, B.H. Kim, Preparation and characterization of Al-doped ZnO transparent conducting thin film by sol–gel processing, J. Korean Ceram. Soc. 33 (1996) 149–154.
[26] C. Cobianu, C. Savaniu, P. Siciliano, S. Capone, M. Utriainen, L. Niinisto, SnO_2 sol–gel derived thin film for integrated gas sensors, Sens. Actuators B: Chem. 77 (2001) 496–502.
[27] O. Singh, M.P. Singh, N. Kohli, R.C. Singh, Effect of pH on the morphology and gas sensing properties of ZnO nanostructures, Sens. Actuators B: Chem. 166 (2012) 438–443.
[28] O. Lupan, L. Chow, G. Chai, H. Heinrich, Fabrication and characterization of Zn–ZnO core–shell microspheres from nanorods, Chem. Phys. Lett. 465 (2008) 249–253.
[29] X.B. Ji, W.C. Lu, H.P. Ma, Photoluminescent hierarchical ZnO microflower and its surface wettability, Cryst. Res. Technol. 47 (2012) 1121–1126.
[30] S.A. Khayyat, M.S. Akhtar, A. Umar, ZnO nanocapsules for photocatalytic degradation of thionine, Mater. Lett. 81 (2012) 239–241.
[31] M.L. Moreira, G.P. Mambrini, D.P. Volanti, E.R. Leite, M.O. Orlandi, P.S. Pizani, V.R. Mastelaro, C.O. Paiva-Santos, E. Longo, J.A. Varela, Hydrothermal microwave: a new route to obtain photoluminescent crystalline $BaTiO_3$ nanoparticles, Chem. Mater. 20 (2008) 5381–5387.
[32] A. Umar, M.M. Rahman, A. Al-Hajry, Y.-B. Hahn, Highly-sensitive cholesterol biosensor based on well-crystallized flower-shaped ZnO nanostructures, Talanta 78 (2009) 284–289.
[33] A.P. Moura, R.C. Lima, M.L. Moreira, D.P. Volanti, J.W.M. Espinosa, M.O. Orlandi, P.S. Pizani, J.A. Varela, E. Longo, ZnO architectures synthesized by a microwave-assisted hydrothermal method and their photoluminescence properties, Solid State Ion. 181 (2010) 775–780.
[34] P. Mitra, A.P. Chatterjee, H.S. Maiti, ZnO thin film sensor, Mater. Lett. 35 (1998) 33–38.
[35] J.R. Macdonald, Impedance Spectroscopy: Emphasizing Solid Materials and Systems, John Wiley, New York, 1987.
[36] E.F. Owede, A.K. Jonscher, Time- and frequency-dependent surface transport on humid insulators, J. Electrochem. Soc. 135 (1988) 1757–1765.
[37] M.C. Feliciangeli, G. Conte, M.C. Rossi, L. Giorgi, R. Giorgi, N. Lisi, Impedance and modulus spectroscopy of nanocrystalline diamond films, Sens. Actuator B: Chem. 126 (2007) 245–251.
[38] N. Ponpandian, P. Balaya, A. Narayanasamy, Electrical conductivity and dielectric behaviour of nanocrystalline $NiFe_2O_4$ spinel, J. Phys. Condens. Matter 14 (2002) 3221–3237.
[39] P.M. Faia, E.L. Jesus, C.S. Louro, TiO_2:WO_3 composite humidity sensors doped with ZnO and CuO investigated by impedance spectroscopy, Sens. Actuators B: Chem. 203 (2014) 340–348.
[40] N. Al-Hardan, M.J. Abdullah, A.A. Aziz, Impedance spectroscopy of undoped and Cr-doped ZnO gas sensors under different oxygen concentrations, Appl. Surf. Sci. 257 (2011) 8993–8997.
[41] T.P. Hulser, H. Wiggers, F.E. Kruis, A. Lorke, Nanostructured gas sensors and electrical characterization of deposited SnO_2 nanoparticles in ambient gas atmosphere, Sens. Actuators B: Chem. 109 (2005) 13–18.
[42] J. Lee, J.H. Hwang, J.J. Mashek, T.O. Mason, A.E. Miller, R.W. Siegel, Impedance spectroscopy of grain boundaries in nanophase ZnO, J. Mater. Res. 10 (1995) 2295–2300.
[43] M. Xu, Q. Li, Y. Ma, H. Fan, Ni-doped ZnO nanorods gas sensor: enhanced gas-sensing properties, AC and DC electrical behaviors, Sens. Actuators B: Chem., 199, , 2014, p. 403–409.
[44] G. Korotcenkov, B.K. Cho, Ozone measuring: what can limit application of SnO_2-based conductometric gas sensors?, Sens. Actuators B: Chem. 161 (2012) 28–44.
[45] M. Epifani, S. Capone, R. Rella, P. Siciliano, L. Vasanelli, G. Faglia, P. Nelli, G. Sberveglieri, In_2O_3 thin films obtained through a chemical complexation based sol-gel process and their application as gas sensor devices, J. Sol-Gel Sci. Technol. 26 (2003) 741–744.
[46] M. Bendahan, R. Boulmani, J.L. Seguin, K. Aguir, Characterization of ozone sensors based on WO_3 reactively sputtered films: influence of O_2 concentration in the sputtering gas, and working temperature, Sens. Actuators B: Chem. 100 (2004) 320–324.
[47] A.S.M.I. Uddin, U. Yaqoob, D.T. Phan, G.S. Chung, A novel flexible acetylene gas sensor based on PI/PTFE-supported Ag-loaded vertical ZnO nanorods array, Sens. Actuators B 222 (2016) 536–543.
[48] V. Galstyan, E. Comini, C. Baratto, G. Faglia, G. Sberveglieri, Nanostructured ZnO chemical gas sensors, Ceram. Int. 41 (2015) 14239–14244.
[49] K. Narimani, F.D. Nayeri, M. Kolahdouz, P. Ebrahimi, Fabrication, modeling and simulation of high sensitivity capacitive humidity sensors based on ZnO nanorods, Sens. Actuators B 224 (2016) 338–343.
[50] X. San, G. Wang, B. Liang, Y. Song, S. Gao, J. Zhang, F. Meng, Catalyst-free growth of one-dimensional ZnO nanostructures on SiO_2 substrate and in situ investigation of their H2 sensing properties, J. Alloy. Compd. 622 (2015) 73–78.
[51] N.F. Hamedani, A.R. Mahjoub, A.A. Khodadadi, Y. Mortazavi, Microwave assisted fast synthesis of various ZnO morphologies for selective detection of CO, CH_4 and ethanol, Sens. Actuators B: Chem. 156 (2011) 737–742.
[52] M. Akermi, N. Sakly, R.B. Chaabane, H.B. Ouada, Effect of PEG-400 on the morphology and electrical properties of ZnO nanoparticles application for gas sensor, Mater. Sci. Semicond. Process. 16 (2013) 807–817.
[53] D.O. Scanlon, A. Walsh, B.J. Morgan, M. Nolan, J. Fearon, G. W. Watson, Surface sensitivity in Li-doping of MgO: a density functional theory study with correction for on-site coulomb interactions, J. Phys. Chem. C 111 (2007) 7971–7979.